IEEE Access
Multidisciplinary | Rapid Review | Open Access Journal

Received 16 August 2022, accepted 25 August 2022, date of publication 12 September 2022, date of current version 20 September 2022.

Digital Object Identifier 10.1109/ACCESS.2022.3205732

RESEARCH ARTICLE

Modeling and Control Design for an Autonomous Underwater Vehicle Based on Atlantic Salmon Fish

SHUBHAM SINGH[1,2,*], SAOOD AHMAD[1,*], SYED MUHAMMAD AMRR[1,3], (Graduate Student Member, IEEE), SALEEM ANWAR KHAN[1], NAZRUL ISLAM[4], ABDULLATIF ABDULHADI GARI[4], AND ABDULLAH A. ALGETHAMI[5], (Member, IEEE)

[1]Department of Mechanical Engineering, Zakir Husain College of Engineering and Technology, Aligarh Muslim University, Aligarh 202002, India
[2]Discipline of Mechanical Engineering, Indian Institute of Technology Gandhinagar, Palaj, Gandhinagar, Gujarat 382055, India
[3]Department of Electrical Engineering, Indian Institute of Technology Delhi, New Delhi 110016, India
[4]Department of Mechanical Engineering, King Abdulaziz University (KAU), Jeddah 21589, Saudi Arabia
[5]Mechanical Engineering Department, Faculty of Engineering, Taif University, Taif 21944, Saudi Arabia

Corresponding author: Syed Muhammad Amrr (syedamrr@gmail.com)

This work was supported by the Deanship of Scientific Research (DSR), King Abdulaziz University, Jeddah, Saudi Arabia, under Grant D-265-135-1443.

*Shubham Singh and Saood Ahmad contributed equally to this work.

ABSTRACT Biologically inspired autonomous underwater vehicles (AUVs) or biomimetic AUVs are made to replicate the structural and physiological features of aquatic species. Thus, incorporation of its design in AUV modelling provides higher efficiency at low speeds and improves maneuverability and controllability. This paper develops a biomimetic AUV design based on structural parameters and physiology of an adult Atlantic Salmon fish and proposes a robust control scheme for propelling the fins. For the biomimetic model design of AUV, a 3D CAD model is developed using the actual parameters of Atlantic Salmon fish. The hydrodynamic analysis is performed to calculate the effect of different angles of fin orientations on the value of drag and lift coefficients. Further, kinematic analysis of the tail propulsion system is carried out using the Denavit Hartenberg convention in the Matlab®. Based on the obtained modeling parameters of AUV, a robust sliding mode controller is proposed for tracking the desired tail propulsion response using a DC motor under model uncertainties and disturbances. Moreover, the closed-loop asymptotic stability is also guaranteed through Lyapunov theory, which ensures the convergence of system states to the desired angular movement. Lastly, the proposed algorithm is validated using simulation results with comparative performance analysis to illustrate its efficacy.

INDEX TERMS Bio-inspired underwater robotics, Solidworks, MatlabVRML, Lighthill slender body theory, tracking control design, robust control.

I. INTRODUCTION

There is a growing interest in the research of autonomous underwater vehicles (AUVs) with an emphasis on mechanical and control system design. Another reason for the popularity of such vehicles is their widespread usage in different tasks, such as marine scientific research, military operations, ecology and water environmental investigations, and oil and gas extraction on the seabed. Due to unpredictability and danger, deep water exploration is a challenging endeavor. Thus, it has drawn the attention of academics and researchers to solve the scientific and technical issues related to the dangerous and unstructured undersea environment. Nonetheless, unmanned underwater vehicle (UUV) applications are not only limited to deep sea explorations. Other applications include exploration in shallow water environments of rivers and lakes, etc., for inspection and collection of samples for experimentation related to microbes and algae research. This has inspired the design of small UUVs, with the main aim of its low-cost fabrication and extending its operational ability [1].

The associate editor coordinating the review of this manuscript and approving it for publication was Shihong Ding.

The underwater vehicle is broadly classified as a manned underwater vehicle (MUV) and an unmanned underwater vehicle (UUV). The UUV category is further classified into remotely operated vehicles (ROV) and autonomous underwater vehicles (AUV) [2], [3]. An AUV has impeccable features, including travel easily at slow and fast speeds and longer mission hours. Further, precise maneuverability and navigation are now also an integral part of AUVs. However, the problem with existing propeller-based systems of AUVs is that they are modeled to work effectively for a specific task that requires cruising at higher speeds. As a result, it renders inefficient performance. Also, these systems have poor maneuverability at low speed, large turning radius, and insufficient control. Researchers have taken up significant research work related to optimization of the propeller-based system for implementation in numerous applications.

In general, robotic fish are classified by their propulsive mode, which varies according to the percentage of lateral movement of their bodies. In [4], twelve different types of swimming are defined. The main challenge in robotic fish modelling is designing a mechanism that reproduces these swimming modes accurately and efficiently. In earlier research, multiple links were used to model the fish, and separate dc motors control all these links. All these links constitute the shape of the tail. Some of the examples of a multi-link motor controlled system include a multi-locomotive robotic fish by Phongchai Nilas [5] and robofish by Anderson *et al.* [6]. Multi-link motor control offers a high degree of freedom, but a large number of motors make the control design complex. Another mechanism is the multi-link rotary shaft, and few examples of a multi-link rotary shaft are the Tunabot by Zhu *et al.* [7], iSplash fish by Clapham and Hu [8], [9]. This system mechanism enables faster speeds and higher frequencies than the system with several servo motors. However, it is hard to implement when engaged with underwater flora and fauna. Later, MIT researchers also created a soft compliant tail using fluidic actuators [10], but it is incapable of recreating the sigmoid-like tail shape, resulting in a relatively slow and inefficient system.

Recently, a more efficient propulsion system is required to improve the performance and endurance of these vehicles. An alternative to existing propeller-based systems is the nature inspired system, i.e., a bio-mimetic propulsion system that is efficient and has an excellent performance in the underwater environments [11]. Lately, the research focus of AUVs has been on the efficient maneuvering abilities of biomimetic fish, which is done by imitating the natural locomotion of fish. As a result, it allows the ability to swim fast with excellent efficiency and ensuring skillful maneuvering in confined spaces. It also has genuine fish abilities, such as turning quickly to capture prey and dodging obstacles [12]. The main reason behind choosing fish-inspired locomotion for underwater vehicles is that fishes and other aquatic animals are efficient swimmers. They possess high maneuverability and can follow trajectories, stabilize themselves efficiently in currents and surges, create fewer wakes compared to other underwater vehicles, and have quiet propulsion. The caudal fin and paired pectoral fins are primarily responsible for the locomotion of fish. Based on locomotion, they are classified into the median and paired pectoral fins (MPF) and body caudal fins (BCF). The investigation of admiringly fast and efficient maneuvering of fish can open the doors for better thruster design and modeling of AUVs dynamics. There is only a little research on the development of AUVs inspired by fish, where fish robots use fins instead of thrusters [13], [14].

The motion control of a biomimetic fish is also an essential aspect of such robots, and the movement of soft tail achieves this propelling swimming motion in the forward direction. Yaw motion can be controlled by maintaining greater fluidic volume in one fish half than the other. By changing the angle of attack of diving planes, the pitch can be regulated. The tail's forward swimming speed influences both yaw and pitch control actions. Absolute attitude readings are provided via an onboard inertial measurement device with 9 degrees of freedom. These measurements are then used to design closed-loop attitude control for robotic fish [15]. The objective of tracking control of a biomimetic fish is to track a route in space specified by a time function starting from a predetermined initial state. It can also include following a moving target point [16]. Many researchers are now working on controller design for path-tracking of biomimetic robotic fish, primarily focused on creating an energy consumption model by examining the dynamics and motion traits of bio-inspired fish and determining the link between behavior and energy consumption.

Due to the complex underwater environment as well as the high coupling and nonlinear properties of bio-inspired robotic fish, underwater path tracking control design is more tedious than other environmental control. In recent years, few control strategies have been implemented for the controller design biomimetic underwater fish, such as PID control, sliding mode control, auto disturbance rejection control, fuzzy logic control, line-of-sight method, etc. The conventional PID control approach is applied in [17] for the attitude tracking problem. However, to deal with challenging fish dynamics and uncertain underwater surroundings, PID control is not always an appropriate method because of the complexity of PID control parameter tuning. Consequently, this makes it ineffective for the multi-objective optimization of complex MIMO control systems. To ensure the invariance against model uncertainties and disturbances, sliding mode control [18], [19], [20] and auto disturbance rejection control [21] schemes are developed. Moreover, fuzzy logic control [22], quantized fuzzy tracking control with event-trigger approach [23], H_∞ control [24], the line-of-sight approach [25], [26], model predictive control [27] are among a few more control techniques employed to regulate robotic fish movements. Although the above-said strategies for the AUV system track the desired path with acceptable state response, their performance may get deteriorated under the influence

of parametric uncertainties and external disturbances. Further, the robust control schemes have only ensured the uniformly ultimate bounded convergence, which can be further improved.

In view of the aforementioned literature, this paper has attempted to develop the underwater vehicle model, including the design, modelling, and motion control of an AUV-based Atlantic Salmon Fish.

The key features of this work is discussed below:

- This paper investigates the highly efficient locomotion mechanisms of adult Atlantic Salmon fish for the potential advantages of utilizing a biomimetic propulsion system for underwater vehicle design. In this regard, the undulation motion of the fish body to propel forward is studied by replicating it with two revolute joints to obtain the undulation gait of the tail of the real fish.
- A 3D CAD model is prepared for a biomimetic model of Atlantic Salmon fish as per scale using SolidWorks.
- The effect of fin orientations is investigated on the different lift and drag coefficient values.
- The governing equations of the tail propulsion system are generated, and its kinematic analysis is done using Denavit-Hartenberg (D-H) convention.
- Based on the actuator parameters of the DC motor, a robust sliding mode control law is proposed for the desired joint motion of fish under model uncertainties and disturbances. The overall closed-loop stability is also established using Lyapunov theory, which guarantees the finite time convergence of sliding surface and asymptotic convergence of angular motion.
- The comparative analysis using simulation results illustrates the superiority of the proposed control scheme.

The paper is organized as follows. Section II describes the Atlantic Salmon fish system and gives its CAD design. Section III presents the CFD analysis of the fish model. In Section IV, the tail propulsion system is discussed, and Section V demonstrates the Denavit-Hartenberg (D-H) representation for the kinematic analysis. The proposed robust controller for the DC motor and its stability is presented in Section VI and Section VII, respectively. Then, Section VIII shows the controller performance using simulation analysis. The paper ends with the concluding remarks in Section IX.

II. SYSTEM MODEL

This paper proposes the design and dynamic modelling of a bio-inspired underwater robotic fish based on Atlantic Salmon fish as a three-link planar manipulator. The body of the fish is divided into three parts, i.e., posterior, anterior, and caudal fin. As Atlantic Salmon fish is a Sub-Carangiform fish, the undulation motion is carried out by oscillating 2/3rd of its body length with the initiation of the undulation from the joint between the posterior part and the caudal fin. The Anterior part is connected to the posterior part with the help of a revolute joint, similarly to the posterior part to the caudal fin. The CAD modelling of the fish is based on its blueprints, which is shown in Figure 1. The 3D CAD model of Salmon

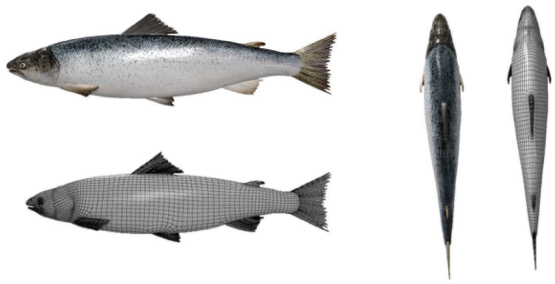

FIGURE 1. Blueprints of Atlantic Salmon fish.

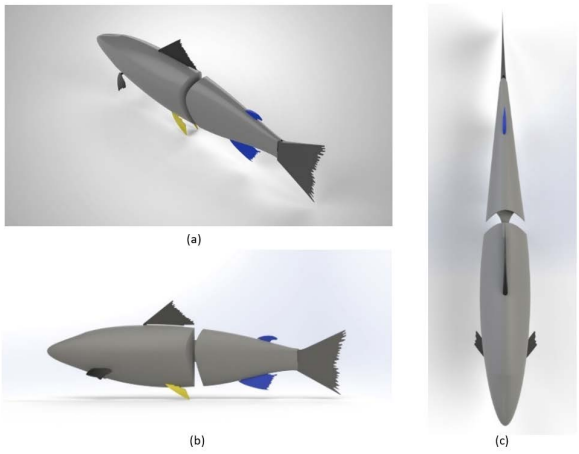

FIGURE 2. CAD design of Atlantic Salmon fish. (a) isometric view (b) front view (c) top view.

Atlantic fish is prepared in the SolidWorks and is illustrated in Figure 2.

A. ANTERIOR BODY DESIGN

The anterior region of biomimetic fish is assumed and designed to be rigid. The argument in favor of this assumption is that the skull bone majorly constitutes it. Additionally, the front half of the fish does not actively undulate. Thus, whatever intrinsic biological flexibility it may have may be safely disregarded for design and analysis needs without significantly changing the fish dynamics.

B. POSTERIOR BODY DESIGN

The posterior region design is more complex than the anterior region. The caudal fin attached to the posterior region is responsible for producing propulsion. The rear body of the vehicle is joined to the caudal fin with the help of a revolute joint (1 DOF). The rear body is assumed and designed to be rigid as to the flexible body of the real fish. The revolute joint is regarded as the active joint because it actively engages in a sinusoidal motion that resembles an undulating wave and passively actuates the movement of the caudal fin to produce propulsion. Thus, the flexibility between the rear portion and the caudal fin is provided by this joint.

C. CAUDAL FIN DESIGN

The caudal fin inspired by the Atlantic Salom fish is attached at the rear end of the bio-inspired robot. It is known that the caudal fin of Atlantic Salmon type fish is homocercal, i.e., it has a truncated shape [28]. The assembled model is shown with all fins attached in the Figure 2. However, for this study, only the caudal fin (tail fin) is participating in the thrust generation, and it is assumed that all other fins have no role.

III. CFD MODELING

The robotic fish's profile is similar to the NACA 0014 airfoil's aerodynamic profile. As the vehicle moves in an undulatory motion, this profile helps to improve swimming efficiency by minimizing drag. Using Lighthill's light wave theory [29], the robotic fish is made to undulate at various angles. As mentioned in this paper [30], the major objective of overcoming drag in powered swimming requires fishes to generate thrust. In the present study, CFD simulation will be used to determine a perfect design and locomotion for a robotic fish vehicle with energy-efficient, lower drag, and improved driving efficiency. Using the ANSYS Fluent software platform, the software contains a broad range of physical modeling capabilities necessary for the present study. The CFD solver is used to solve the Navier-Stokes equation. As per the conservation of momentum principle, the finite volume formulation for an incompressible Newtonian fluid is given as

$$\rho(\partial V/\partial t) = F - \Delta p + \mu \Delta^2 V \tag{1}$$

$$\Delta . V = 0 \tag{2}$$

where V represents the velocity, ρ is the density of fluid, Δp is the pressure, $\partial V/\partial t$ is the partial derivative w.r.t. t, F represents the force acted on the body, μ is the dynamic viscosity of the fluid. The CFD simulations are carried out systematically to calculate numerous factors impacting the flow characteristics.The simulation steps are summarised in the following brief manner:

1) A discretized mesh is prepared using ANSYS Meshing. The tetrahedral mesh has been prepared with a minimum element size of 0.001mm and a target skewness of 0.8. The inflation ratio is 0.272 with maximum inflation layers five, and the growth ratio is 1.2.
2) The three-link robotic fish CFD model is set up in the ANSYS CFD module. The method used is laminar, and cell zone conditions are fluid: water, and solid body: ABS. Boundary conditions are inlet velocity: 5m/s, outlet gauge pressure: 0 pa, mesh motion: moving domain, pressure: second-order, momentum: second order upwind, transient formulation: first-order implicit. Numerical scheme used: coupled.
3) Comparative and comprehensive analysis of the different kinematic parameters like the amplitude span and the tail beat frequency with hydrodynamic factors like Cd (drag coefficient) and Cl (Lift coefficient) is carried out. Drag and lift coefficients are determined by changing the inclination angle of the rear body and caudal fins to match with that the swimming motion of the fish.
4) Pressure, velocity distribution contours, and velocity streamline are also investigated and discussed.

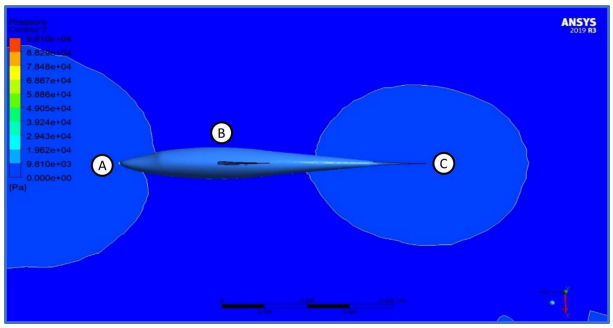

FIGURE 3. Pressure contour at mean position ($t = 0$).

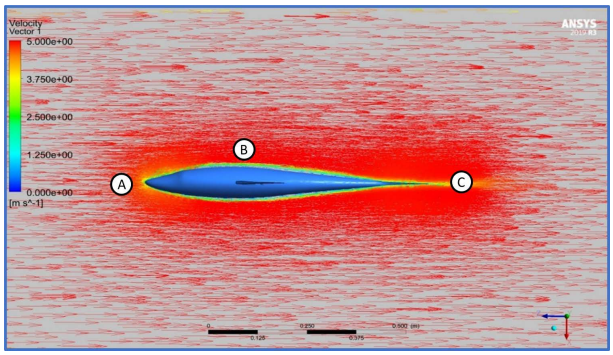

FIGURE 4. Velocity vector at mean position ($t = 0$).

The idea of dynamic meshing is effectively employed in this project. A steady mesh is employed in CFD simulations to take that the physical geometry remains constant. Dynamic meshing, on the other hand, is a necessary aspect of modelling for moving geometries. The challenges faced during the body's dynamic meshing include parameter selection linked to cell height and solver discovered divergence (pressure correction). Furthermore, negative cell volumes were discovered when the dynamic mesh update failed multiple times, along with minor issues such as simulation time step smoothing, etc.

A. MEAN POSITION

In Figure 3, the pressure contour is shown at the mean position when $t = 0$. The posterior body (caudal fin) begins to move (starting from rest) in either direction (left or right) when the fish initiates the locomotion. A high-pressure region is observed in the anterior region (A) and the posterior region (C) of the fish. The region (B) has a lower pressure region than regions A and C. Similarly, in Figure 4, the velocity vector is shown at the mean position when $t = 0$. Velocity difference can be seen in region-A, followed by region B, and at the fin end (region C). In Figure 5, the velocity streamline

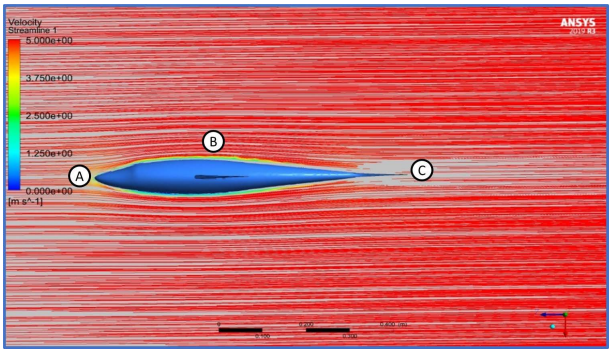

FIGURE 5. Velocity streamline at mean position (t=0).

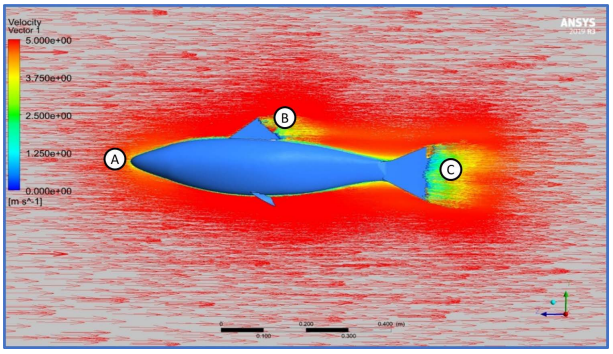

FIGURE 6. Velocity streamline (front view) at mean position ($t = 0$).

is shown at mean position when $t = 0$. It can be observed that the flow is streamlined throughout the entire body of the fish, as seen from the top view. In the front view (Figure 6), flow separation can be seen at the trailing edge of the dorsal fin (region B) and after the caudal fin (region C) due to restriction offered to the flow by these fins.

B. INITIATION OF UNDULATING MOTION

In Figure 7, the pressure contour, when the posterior region of the fish starts undulating in the clockwise direction (10 degrees), is shown. The posterior body (caudal fin) begins to initiate the undulating locomotion of the fish. A high-pressure region is observed in the anterior region (A) and the posterior region (C) of the fish. Initially, the flow was allowed to stabilize, following which the results were obtained and analyzed. On the right side, observed the high pressure and on the left side, there is a low pressure (region C). Even though the tail is moving towards the left from the mean position, positive pressure is generated on the right side because the tail pushes the flow to the left. When the rear part of the body (posterior region) moves to the left position completely (10 degrees), it can be seen in region-C that the magnitude of the pressure on the right side is higher than those on the left. Also, as seen from the figure in region D, a high-pressure region between the anterior and posterior body. In Figure 8, the velocity vector is shown when the posterior region of the fish starts undulating in the clockwise direction (10 degrees).

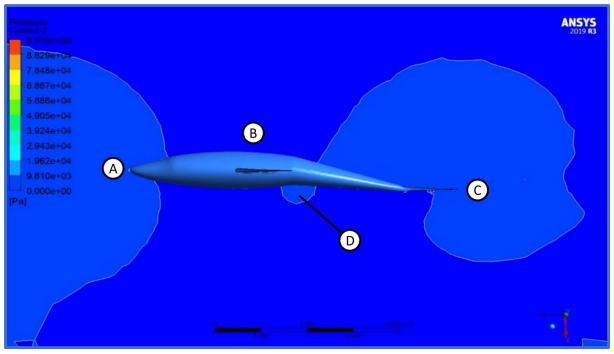

FIGURE 7. Pressure contour for Undulating motion of posterior body at frequency 0.5 Hz and angle Amplitude 10 degree (CW).

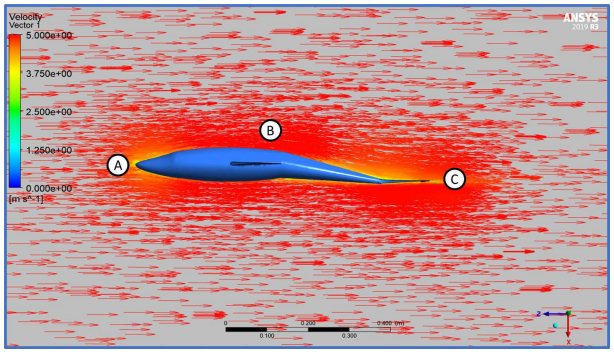

FIGURE 8. Velocity vector for undulating motion of posterior body at frequency 0.5 Hz and angle amplitude of 10 degree (CW).

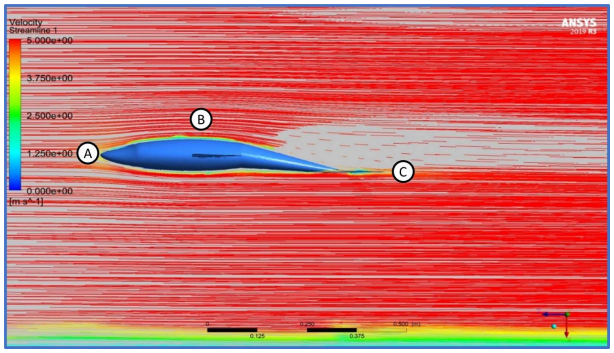

FIGURE 9. Velocity streamline for undulating motion of posterior body at frequency 0.5 Hz and amplitude of 10 degree (CW).

The velocity vectors vary with higher magnitudes in regions A and C and lower magnitudes in region B. In Figure 9, the velocity streamline is shown when the posterior region of the fish starts undulating in the clockwise direction (10 degrees). It can be seen that the flow is streamlined till the end of the anterior body (regions A and B). It starts to separate from the posterior body onwards, thus leading to flow separation and vortex formation in region C.

In Figure 10, the pressure contour is shown when the rear part of the body (posterior region) of the fish starts undulating in the counterclockwise direction (10 degrees). The posterior

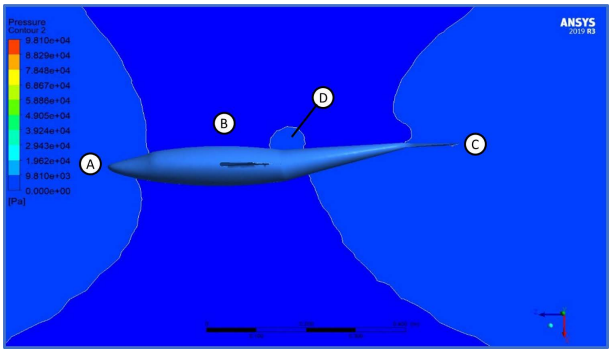

FIGURE 10. Pressure contour for undulating motion of posterior body at frequency 0.5 Hz and angle 10 degree (CCW).

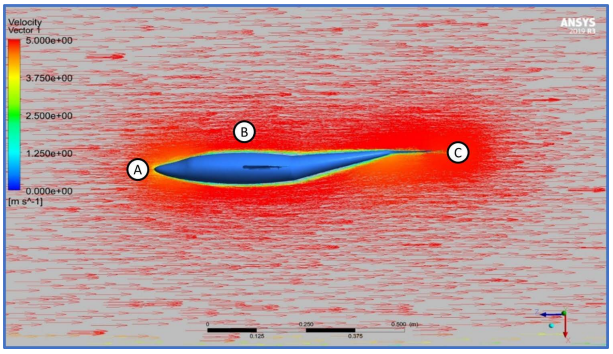

FIGURE 11. Velocity vector for undulating motion of posterior body at frequency 0.5 Hz and angle 10 degree (CCW).

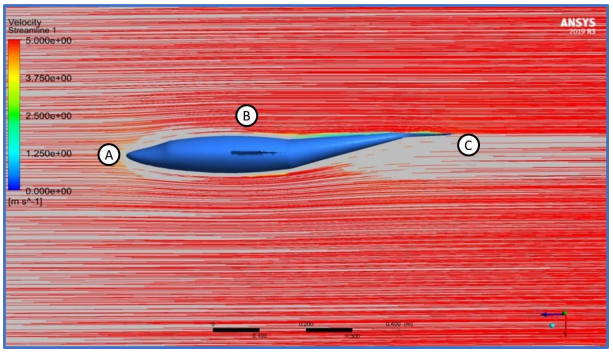

FIGURE 12. Velocity streamline for undulating motion of posterior body at frequency 0.5 Hz and angle 10 degree (CCW).

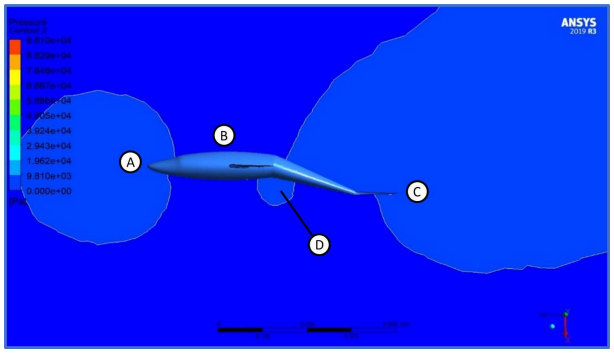

FIGURE 13. Pressure contour for undulating motion of posterior body at frequency 0.5 Hz and angle 20 degree (CW).

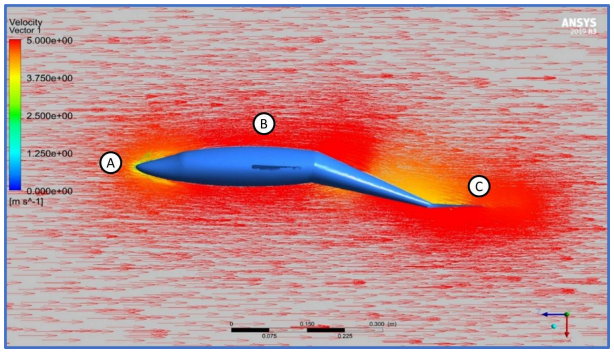

FIGURE 14. Velocity vector for undulating motion of posterior body at frequency 0.5 Hz and angle 20 degree (CW).

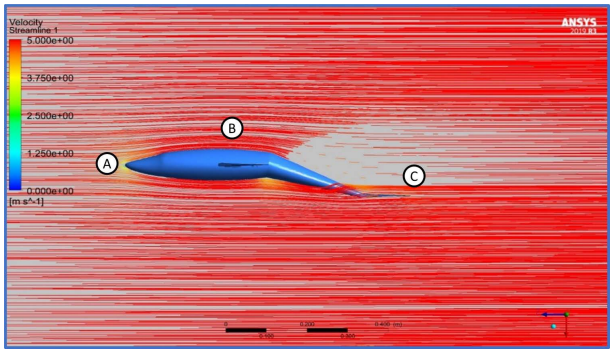

FIGURE 15. Velocity streamline for undulating motion of posterior body at frequency 0.5 Hz and angle 20 degree (CW).

body's position (caudal fin) first returns to its mean position from the 10-degree CW position and starts moving 10 degrees towards the right (CCW). A high-pressure region is observed in the anterior region (A) and the posterior region (C) of the fish. On the right side, high pressure is observed, and on the left, there is low pressure. As the tail is moving from the mean position to the right, it pushes the flow to the right, generating high pressure on the left side of region-C. When the rear part of the body (posterior region) moves to the left completely (10 degrees), it can be seen that the pressure magnitudes on the left side are higher than on the left side. In Figure 11, it is also shown that the high pressure area is concentrated in the region-D near the posterior body of the fish. In Figure 11, the velocity vector is shown when the posterior region of the fish starts undulating in the counterclockwise direction (10 degrees). The high pressure gradient creates an intense velocity vector field surrounding the body. These velocity vectors constantly vary with larger magnitude in regions A and C and smaller magnitude in region B. In Figure 12, the velocity streamline is shown when the posterior region of the fish starts undulating in the counterclockwise direction (10 degrees). It can be seen that the flow is streamlined till the end of the anterior body (regions A and B). It starts to separate from the posterior region onwards (same

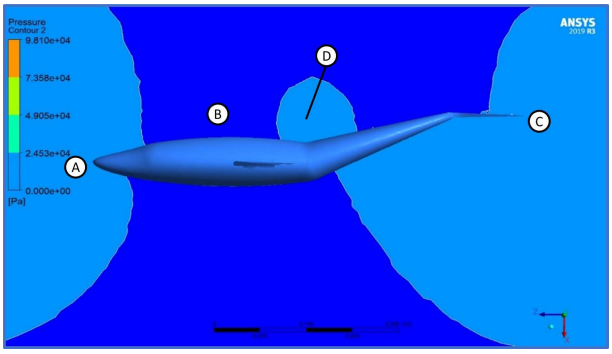

FIGURE 16. Pressure contour for undulating motion of posterior body at frequency 0.5 Hz and angle 20 degree (CCW).

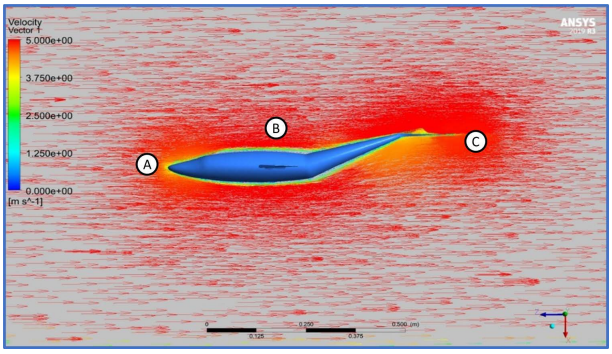

FIGURE 17. Velocity vector for undulating motion of posterior body at frequency 0.5 Hz and angle 20 degree (CCW).

as CW direction), thus, leading to flow separation and vortex formation in region C.

C. UNDULATING MOTION

In the Figure 13, the pressure contour when the posterior region of the fish starts undulating in the clockwise direction (20 degrees) is shown. The posterior body's position (caudal fin) first returns to its mean position from the 10 degree CCW position and starts moving 20 degrees towards the left (CW). A high-pressure region is observed in the fish's anterior region (A) and posterior region (C and D). The magnitude of the high pressure for the given condition is greater than the previous condition (10 degrees in both directions). Even though the tail is moving towards the left from the mean position, pushing the flow towards the left, which generates high pressure on the right side.

When the rear part of the body (posterior region moves) to the left completely (20 degrees), it can be seen that the magnitudes of pressure on the right side are higher than those on the left. In Figure 13 is shown that, the high pressure area is concentrated around the posterior region. In Figure 14, velocity vector is shown. The pressure gradient creates a velocity vector field surrounding the body. These velocity vectors vary constantly with larger magnitudes (higher than the previous condition of 10 degrees) in regions A and C and smaller magnitudes in region B. In Figure 15, velocity streamline is shown when the posterior region of the fish

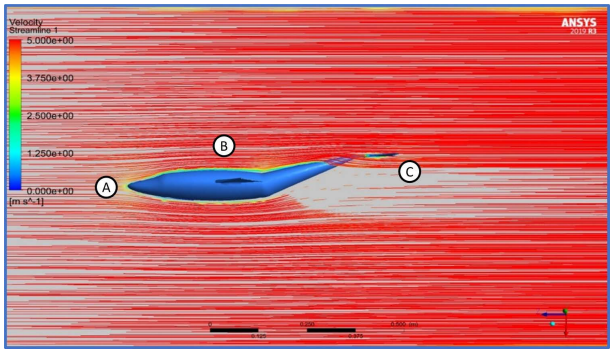

FIGURE 18. Velocity streamline for undulating motion of posterior body at frequency 0.5 Hz and angle 20 degree (CCW).

starts undulating in the Clockwise Direction (20 degrees). It can be seen that the flow is streamline till the end of the anterior body (regions A and B). It starts to separate from the posterior region in region C, thus leading flow separation and vortex formation.

In Figure 16, the pressure contour when the posterior region of the fish starts undulating in the Counter clockwise direction (20 degrees) is shown. The position the posterior body is in (caudal fin) first return to its mean position from the 20 degree CW position and starts moving 20 degrees towards left (CCW). A region of high pressure is observed at the anterior region (A) of the fish starting from the nose of the fish as well as at the posterior region of the fish (C).

When the rear part of the body (posterior region) moves to the right completely (20 degrees), it can be seen that the magnitude of pressure is higher on the left as compared to the right side. In Figure 16, it is shown that the high pressure area is concentrated near the rear part of the body (posterior region) of the fish (regions C and D). In Figure 17, velocity vector is shown. The high pressure gradient creates an intense velocity vector field surrounding the body (regions A, B, and C). These velocity vectors vary constantly with larger magnitude (higher than the previous condition of 10 degrees in both directions) on the left side and smaller magnitudes on the right side of the rear part of the body (posterior region). In Figure 18, the velocity streamline is shown when the posterior region of the fish starts undulating in the counterclockwise direction (20 degrees). It can be seen that the flow is streamline till the end of the anterior body (regions A and B), and it starts to separate from the posterior region onwards (region C), thus leading to flow separation and vortex formation.

D. TAIL BEAT FREQUENCY EFFECTS

It is observed that raising the body wave's amplitude causes the pressure field and velocity vectors to grow proportionally along the tail fin (caudal region). It is also observed that as the caudal region undulates via the intermediate point to the extreme position, the pressure differential between the body's two sides also decreases [31]. The vortex formation near the caudal region is due to the pressure difference.

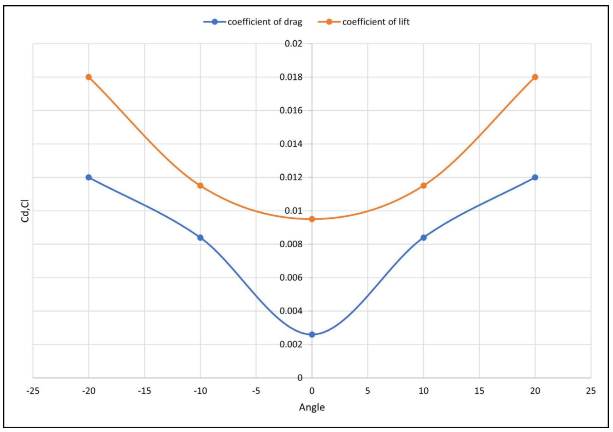

FIGURE 19. Plot of Cd, Cl Vs Angle of attack.

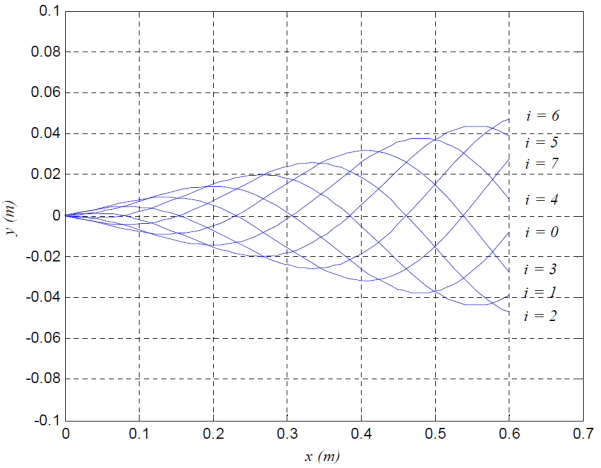

FIGURE 20. Fish kinematics using travelling wave equation.

This supports the light hill theory of undulation [29] which states a reactive pressure equilibrium between the body and the fluid (environment) is required for optimal undulatory fish motion. The value of drag and lift coefficients calculated from the simulation for different rear body and caudal fin orientations is plotted, as shown in Figure 19.

IV. TAIL PROPULSION SYSTEM DESIGN

The proposed vehicle propulsion system design through tail motion is discussed in this section. The design is inspired by the undulation motion of fish. The undulation part responsible for generating thrust is based on a two-link planar manipulator arm (2DOF). The origin of the wave occurs at the joint between the tail and fish body. Further, the parameters of the travelling wave change according to the intended swimming motion. When the fish swims, its body is said to resemble the following travelling wave equation closely:

$$y_{\text{body}}(x, t) = (c_1 x + c_2 x^2)\sin(\kappa x + \omega t) \tag{3}$$

Here, y_{body} represents the lateral displacement of a tail unit from the central axis (m), x is displacement along the tail, t is time, κ denotes the body wave number, c_1 and c_2 are the linear and quadratic wave amplitude envelope, respectively, and w is angular frequency. Further, expression (3) can be redefined in the discretized equation as [14], [32]

$$y_{\text{body}}(x, i) = (c_1 x + c_2 x^2)\sin(\kappa x \pm \frac{2\pi}{M} i) \tag{4}$$

for $i = 0, 1, \ldots, M-1$, where i represents the ith variable of the sequences $y_{\text{body}}(x, i)$ $(i = 0, \ldots, M-1)$ in one oscillation period, M is the resolution of the discrete travelling wave.

Figure 20 illustrates the fish kinematics, which is obtained with the help of travelling wave expression (4) with the given parameter values: $c_1 = 0.08$, $c_2 = 0$, $\kappa = 10.2$, and $M = 2$. The Atlantic Salmon fish have $57-60$ vertebrate [33]. These vertebrae are assumed as one degree of freedom joints [14]. In this paper, the proposed model has finite joints, i.e., 2. Manoeuvrability and redundancy can be improved by further addition of links for smooth wave generation [14]. However, the addition of links results in increased complexity, thus making the realization of the tail design challenging [32].

V. DENAVIT-HARTENBERG (D-H) REPRESENTATION

The proposed structure of the vehicle is intended to have 2 revolute (1 DOF) joints, each powered by an individual DC motor. The undulating motion required to move the bio-inspired vehicle is produced by the combined motion of these actuated joints. The location of the joints at particular points in the swimming gait must be established using kinematics to manage the tail motion. Hence, the D-H representation is implemented where each joint is assigned a 2-axis reference frame, as demonstrated in Figure 21. The transformation matrix is given by [34]

$$^{i-1}_{i}T = R_{(x)}(\alpha_{(i-1)})D_x(a_{(i-1)})R_{(z)}(\theta_i)D_{(z)}(d_i) \tag{5}$$

From the transformation matrices in the equation above (frames), the x and y coordinates for each link are obtained.

The homogeneous transformation matrix has the rotation matrix and displacement vectors for the frames. Since our concern is about the end position of the caudal fin (2D planar), we will focus on displacement vectors for the positions and will be neglecting the orientations from the rotation matrix, as 2D orientation does not make sense. The planar fish links are simulated using Denavit-Hartenberg transformation in Matlab. Figure 22 shows the path traced by the caudal fin and rear body.

VI. ROBUST CONTROLLER DESIGN FOR FIN MOTION

The designed model of the fish consists of two joints that constitute the propulsion system. Separate DC motors actuate these joints. Each joint is actuated to a desired angular position so that the combined motion of all joints mimics the undulation exhibited by the real Atlantic Salmon.

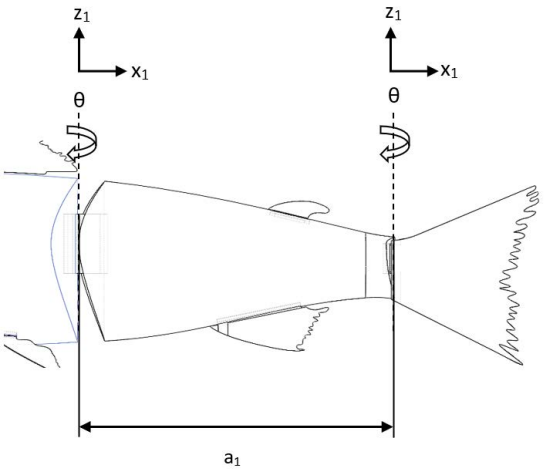

FIGURE 21. Two joint tail configuration.

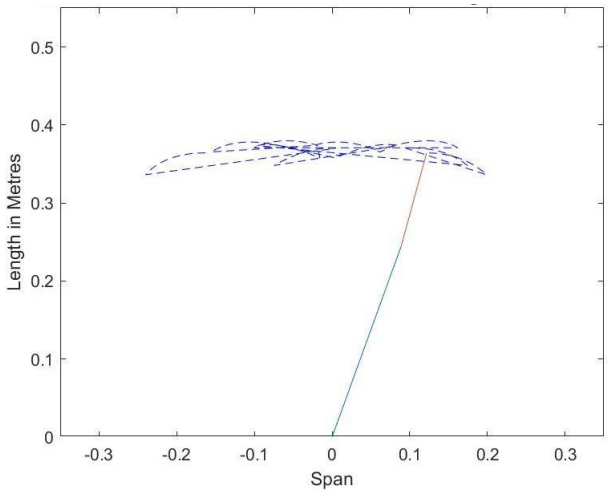

FIGURE 22. Plot of path traced by the caudal fin & rear body for different joint angles.

The dynamic equations of the DC motor are given by [35]:

$$J\ddot{\theta} + \mathcal{B}\dot{\theta} + T_d = Ki \tag{6a}$$
$$L\dot{i} + Ri + K\dot{\theta} = V \tag{6b}$$

where $J > 0$ is the moment of inertia, $\theta \in \mathbb{R}$ is the rotational motion, $\mathcal{B} > 0$ is the coefficient of viscous friction, T_d denotes the external load disturbance, $K > 0$ is the torque coefficient, $i \in \mathbb{R}$ is the armature current, $V \in \mathbb{R}$ is the motor armature voltage, $R > 0$ and $L > 0$ are the armature coil resistance and inductance, respectively.

The above two equations (6) can be rewritten as [36]

$$\dddot{\theta} = -A\ddot{\theta} - B\dot{\theta} + Cu - DT_d - E\dot{T}_d \tag{7}$$

where $A = (JL)^{-1}(JR + \mathcal{B})L$, $B = (JL)^{-1}(\mathcal{B}R + K^2)L$, $C = (JL)^{-1}K$, $D = (JL)^{-1}R$, $E = (JL)^{-1}L$, and $u = V$ is the control input. The parameters $A, B, C \in \mathbb{R}^+$.

Suppose, A, B, and C parameters have model uncertainties, which are denoted as ΔA, ΔB, and ΔC, respectively. Therefore, the system (7) under such model uncertainties can be redefined as

$$\begin{aligned}\dddot{\theta} &= -(A + \Delta A)\ddot{\theta} - (B + \Delta B)\dot{\theta} + (C + \Delta C)u - DT_d \\ &\quad - E\dot{T}_d \\ \dddot{\theta} &= -A\ddot{\theta} - B\dot{\theta} + Cu + \phi\end{aligned} \tag{8}$$

where $\phi = -\Delta A\ddot{\theta} - \Delta B\dot{\theta} + \Delta Cu - DT_d - E\dot{T}_d$.

The third derivative system 8 can be simplified into a single derivative system by using the following state transformation. Let

$$x_1 = \theta;\ x_2 = \dot{\theta};\ x_3 = \ddot{\theta}. \tag{9}$$

Therefore,

$$\dot{x}_1 = x_2, \tag{10a}$$
$$\dot{x}_2 = x_3, \tag{10b}$$
$$\dot{x}_3 = \dddot{\theta} = -A\ddot{\theta} - B\dot{\theta} + Cu + \phi, \tag{10c}$$

where x_1, x_2, and x_3 represent the angular position, angular velocity, and angular acceleration of joint, respectively. An effective controller is needed to turn the DC motor to the proper angular position so that the combined action of each joint results in an undulating movement. The controller should be able to perform the desired motion while rejecting the effects of total disturbances and uncertainties.

While developing the proposed control scheme, the following presumptions are taken into account.

Assumption 1: The states x_1, x_2, and x_3 are measurable.

Assumption 2: The overall uncertainty ϕ is assumed to be bounded such that $|\phi| \leq \bar{\phi}$.

Remark 1: The supporting argument for the boundedness of the uncertainties in Assumption 2 can be explained as follows. First of all, parameters A, B, and C are constituted using physical parameters, such as inductance, resistance, moment of inertia, coefficients of friction, and torque. Since these are all finite values, the uncertainties within A, B, and C are bounded. Secondly, the designed sliding mode-based control law (15) is comprised of finite system parameters and a linear combination of error and system states. Because of the physical limitation of the system, these error and state values are bounded. Also, the actuation of DC motor is subjected to physical limitation, and they can not exceed the maximum limit. Therefore, the control input has a saturation value, which means u is also bounded. Lastly, it is assumed that the external disturbance T_d and its derivative are bounded [36]. Consequently, the overall uncertainties can be considered to be bounded [37].

A. PROBLEM OBJECTIVE

The objective of the proposed controller design is to achieve the desired motion of fish by following the reference trajectory of fin position. In other words, the controller will actuate the desired fin motion in order to track the desired path. Moreover, the proposed controller must also tackle the system

uncertainties and surrounding disturbances while performing the tracking operation [38].

In view of the above statement, suppose x_r be the time-varying reference angular position. The error between the actual and the desired angular position is given as

$$e = x_1 - x_r. \tag{11}$$

Therefore, the relative system dynamics using (10) and (11) can be expressed as

$$\dot{e} = \dot{x}_1 - \dot{x}_r = x_2 - \dot{x}_r, \tag{12a}$$
$$\ddot{e} = \dot{x}_2 - \ddot{x}_r = x_3 - \ddot{x}_r, \tag{12b}$$
$$\dddot{e} = \dot{x}_1 - \dddot{x}_r = -A\ddot{\theta} - B\dot{\theta} + Cu + \phi - \dddot{x}_r. \tag{12c}$$

B. SLIDING MODE CONTROL DESIGN

The sliding mode control (SMC) has been widely used for the robust controller design [39] due to the property of invariance against unknown disturbances and faster convergence time [37], [40], [41], [42], [43], [44]. Therefore, in this paper, SMC is proposed for the motion control of fins through DC motors, which is subjected to model uncertainties and disturbances.

The structure of the sliding surface is selected as

$$s = c_1 e + c_2 \dot{e} + c_3 \ddot{e}. \tag{13}$$

where $s \in \mathbb{R}$, and $c_i \in \mathbb{R} > 0$ for $i = 1, 2, 3$. The time derivative of s yields

$$\begin{aligned} \dot{s} &= c_1 \dot{e} + c_2 \ddot{e} + c_3 \dddot{e} \\ &= c_1 \dot{e} + c_2 \ddot{e} + c_3(-Ax_3 - Bx_2 + Cu + \phi - \ddot{x}_r). \end{aligned} \tag{14}$$

The proposed sliding mode control law is expressed as

$$\begin{aligned} u = \frac{1}{C}\Bigg(Ax_3 + Bx_2 \; + \dddot{x}_r - \frac{c_1}{c_3}\dot{e} - \frac{c_2}{c_3}\ddot{e} - k_1 s \\ -k_2 \,\text{sign}(s)\Bigg). \end{aligned} \tag{15}$$

where $k_1 > 0$ and $k_2 > \bar{\phi} > 0$ are the control gain constants.

VII. STABILITY ANALYSIS

This section demonstrates the stability analysis of the closed-loop control system using the Lyapunov theory. The stability proof employs the following finite time convergence lemma.

Lemma 1: [45], [46]: Consider a continuous system $\dot{\zeta} = f(\zeta) \in \mathbb{R}^n$ with zero being the equilibrium point of $f(\zeta)$ and $\zeta(t_0 = 0) = \zeta_0$. The origin is said to be finite time stable for system $\dot{\zeta}$ if a Lyapunov function $V(\zeta) : \mathbb{R}^n \to \mathbb{R}$ with $\alpha_1 > 0$, $\alpha_2 > 0$, and $\beta \in (0, 1)$ satisfies the following condition

$$\dot{V}(\zeta) + \alpha_2 V(\zeta) + \alpha_1 V^{\beta}(\zeta) \leq 0. \tag{16}$$

Theorem 1: Consider the relative state dynamics (12) under Assumption 1 and 2. The action of the proposed control law (15) will force the sliding surface to zero in finite time and converge the relative system states to zero asymptotically.

Proof: Consider a Lyapunov function $V(s, t)$ as

$$V(s, t) = \frac{1}{2}s^2. \tag{17}$$

The derivative of V with respect to time yields

$$\dot{V}(s, t) = \frac{d}{dt}V(s, t) = \frac{\partial V}{\partial s}\frac{ds}{dt} = \frac{1}{2}(2s)\dot{s} = s\dot{s} \tag{18}$$

Substituting the value of $\dot{s}$ in (19) gives

$$\dot{V} = s(c_1\dot{e} + c_2\ddot{e} + c_3(Cu + \phi - \dddot{x}_r - Ax_3 - Bx_2))$$

Substituting u from (15) in $\dot{V}$ yields

$$\begin{aligned} \dot{V} &= s(\phi - k_1 s - k_2 \,\text{sign}(s)) = s\phi - k_1 s^2 - sk_2 \,\text{sign}(s) \\ &\leq |\phi||s| - k_1 s^2 - k_2|s| \leq \bar{\phi}|s| - k_1 s^2 - k_2|s| \\ &= -k_1 s^2 - \underbrace{(k_2 - \bar{\phi})}_{\bar{k}_2 > 0}|s| = -k_1 s^2 - \bar{k}_2|s| \\ &= -2k_1\frac{s^2}{2} - \sqrt{2}\bar{k}_2\frac{|s|}{\sqrt{2}} \leq -2k_1\left(\frac{s^2}{2}\right) - \sqrt{2}\bar{k}_2\left(\frac{|s|^2}{2}\right)^{1/2} \\ \dot{V} &\leq -\chi_1 V - \chi_2 V^{\frac{1}{2}} \end{aligned} \tag{19}$$

where $\chi_1 = 2k_1 > 0$ and $\chi_2 = \sqrt{2}\bar{k}_2 > 0$. Consequently, the inequality (19) satisfies the finite time condition of Lemma 1. Therefore, the sliding surface s converges to zero within finite time.

Now, once s goes to zero, the sliding surface Equation (13) can be rewritten as

$$\begin{aligned} s = c_1 e + c_2\dot{e} + c_3\ddot{e} = 0 \\ \text{or,} \quad (c_3\varpi^2 + c_2\varpi + c_1)E(\varpi) = 0 \\ c_3\varpi^2 + c_2\varpi + c_1 = 0 \end{aligned} \tag{20}$$

where ϖ is the Laplace variable. Since c_1, c_2, and c_3 are all positive, Equation (20) is a Hurwitz polynomial with positive coefficients. Therefore, the relative state is stable, i.e., e will converge to zero asymptotically. Consequently, the angular position θ will track the desired trajectory θ_r. Hence, the proof of Theorem 1 is completed. □

Remark 2: The key insights which can be taken from the proposed investigation are as follows:

- A biomimetic model of the Atlantic salmon fish will exhibit lower drag. Thus, it will have higher efficiency than a propeller-based underwater vehicle.
- Mimicking a real fish's locomotion can improve the propulsive and maneuvering efficiencies of AUV Design.
- The hydrodynamic and Kinematic analyses give the performance verification of the biomimetic model.
- Since it is difficult to obtain the exact parameter values of the design model; therefore, a robust controller scheme will be required.
- A fast controller scheme, such as the SMC method, will be required to achieve a quick system response with a good transient and steady-state behavior. The controller

will dictate the fin motion according to the desired angular motion.
- In summary, the biomimetic AUV system can be an efficient alternative to the existing propeller-based systems.

VIII. SIMULATION RESULTS WITH COMPARATIVE ANALYSIS

This section presents the simulation performance of the proposed SMC law (15) under model uncertainties and disturbances using numerical analysis. Further, in order to establish the effectiveness of the proposed scheme, two well known control approaches are also implemented for comparative analysis. These two control schemes are: proportional integral derivative (PID) control and feedback linearization (FBL) control [47].

The uncertainties in A, B, and C parameters are considered to be 10%, 15%, and 5% of the nominal value, respectively. The exogenous disturbance is considered as

$$T_d = 0.5\sin(0.5\,t).$$

The reference signal for angular movement is considered to be the sum of sin and cosine function at different frequencies, and it is given as

$$x_r = \theta_r = \sin(0.5t) + \cos(t). \tag{21}$$

A. GEAR RATIO

A high speed DC motor can rotate at thousands of rev/min that can cause rapid movement in the tail part. Therefore, gear systems are used to avoid the fast movement by reducing the speed and increasing the motor torque production [48]. Figure 23 shows the gear train between the motor and load that gives the change in the angular movement at the load side θ_L and the motor side θ_m. In this work, the gear ration is considered as $n = 298:1$, which means the driver gear rotates 298 revolutions to turn the driven gear 1 revolution [35]. The physical parameters of the DC motor, gear system, and proposed controller are presented in Table 1.

B. SIMULATION PERFORMANCE

The numerical results of the proposed and comparative control designs are demonstrated from Figure 24 to Figure 27. The DC motor drives the angular movement of joint θ or x_1 to track the desired reference signal θ_r or x_r. Figure 24 shows that the trajectory of θ under different schemes tracks a time and amplitude varying reference signal. However, the proposed scheme has a faster convergence time, as is evident from Figure 24. The convergence response can also be visualized through the error state trajectory plot, which is demonstrated in Figure 25. One can observe from this figure that the error converges to the bound of zero quicker under the proposed scheme as compared to the other two schemes. The convergence time of error e under different schemes are depicted in Table 2. Moreover, the tracking error

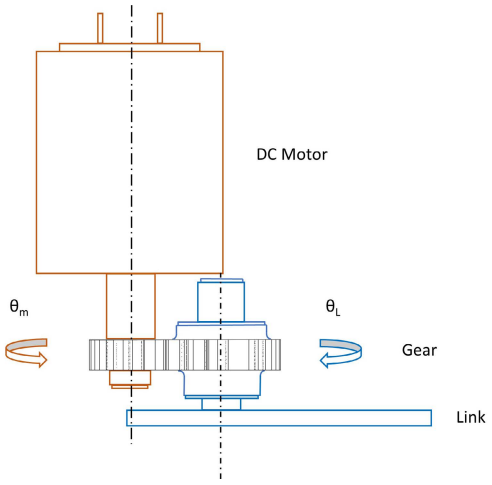

FIGURE 23. Schematic diagram of revolute joint.

TABLE 1. System and proposed control parameters.

Para.	Value	Para.	Value	Para.	Value
R	7 Ω	J_L	0.022 kg-m^2	c_2	5
L	1.3 mH	$\mathcal{B}_L$	0.0005N-m-s/rad	c_3	0.3
J_m	0.022 kg-m^2	K	0.04N-m/amp	k_1	2000
$\mathcal{B}_m$	0.0030N-m-s/rad	c_1	20	k_2	3.8

performance of these three control schemes is also evaluated using the measures of integral of square error (ISE), integral of absolute error (IAE), integral of time square error (ITSE), and integral of time absolute error (ITAE). The expression of these performance measure can be seen from [49]. The values of these performance measures are tabulated in Table 2, which clearly shows that the proposed scheme has a minimum value in all the error measures as compared to the other two methods. Therefore, the proposed robust SMC scheme performs best under multiple uncertainties and provides a faster convergence with better error measures.

Figure 26 illustrates the sliding surface response of the proposed scheme where the sliding mode phase is achieved in 1s. Once the sliding phase is attained, the surface remains at this mode for the whole time. The control input response of these three control schemes is shown in Figure 27. Initially, all the three control schemes have a high magnitude of input response. The large input effort is required to rapidly attain the desired reference signal. Once the desired angle

TABLE 2. Performance measures under different control schemes.

Measures	PID	FBL	Proposed
$\mathbf{T_{settling}}$ **of** e	2.056 s	2.641 s	1.011 s
ISE	0.2554	0.6219	0.1792
IAE	0.7110	0.9205	0.3396
ITSE	0.1246	0.2379	0.0252
ITAE	3.3776	1.0609	0.8406

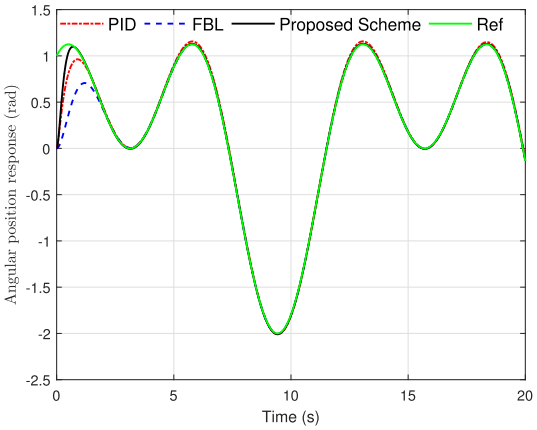

FIGURE 24. Angular position responses of DC motor under different schemes with respect to the reference trajectory.

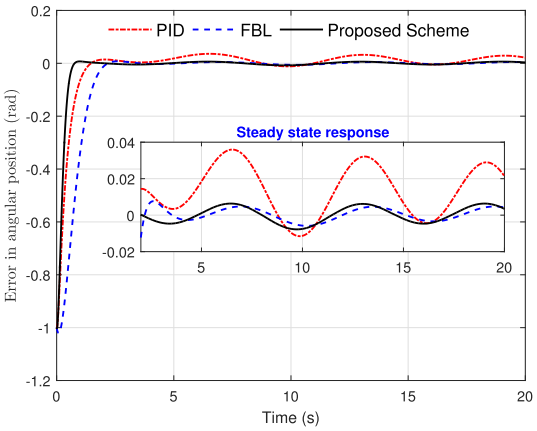

FIGURE 25. Tracking error responses under different control schemes.

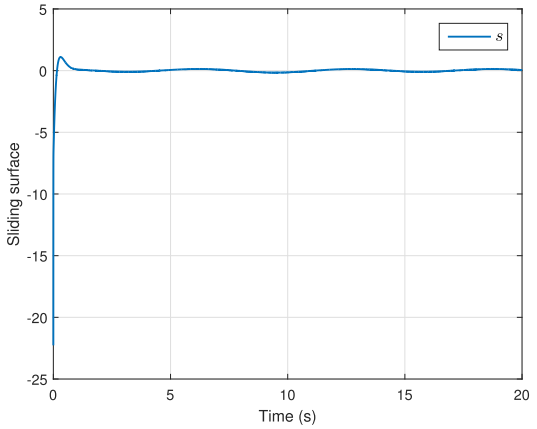

FIGURE 26. Sliding surface response of the proposed scheme.

is achieved, the control input varies sinusoidally to attain the time varying sinusoidal reference signal and nullify the undesirable model dynamics.

In summary, the proposed algorithm successfully tracks the time-varying reference signal and effectively rejects the disturbance. Moreover, compared with the comparative results, the proposed SMC scheme is performing much better in terms of good transient and steady-state response and error performance measures.

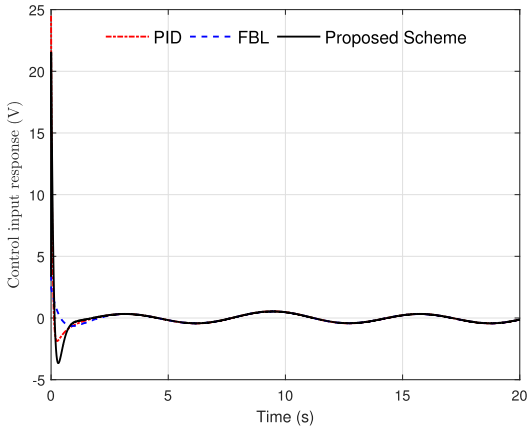

FIGURE 27. Control input responses under different schemes.

IX. CONCLUSION

This paper explores the design, simulation, and mathematical modelling of a biomimetic underwater vehicle, whose design is inspired by an Atlantic Salmon fish. The vehicle moves forward by performing an undulating motion with around half of its body. Two joints are considered in the present design to mimic the undulating tail movement of actual fish. Moreover, a robust SMC scheme is also implemented to the given design model for the fin motion of AUV using a DC motor subjected to the model uncertainties and disturbances. The Lyapunov analysis is carried out to show the asymptotic stability of the relative angular states. Further, the effectiveness of the proposed algorithm is validated using numerical analysis with comparative performance. The next part of this work is to design the 3-dimensional working model based on the modelling analysis and execute the control algorithm.

ACKNOWLEDGMENT

This work was supported by the Deanship of Scientific Research (DSR), King Abdulaziz University, Jeddah, Saudi Arabia, under Grant D-265-135-1443. The authors, therefore, gratefully acknowledge DSR technical and financial support.

REFERENCES

[1] Z. Wang, G. Hang, J. Li, Y. Wang, and K. Xiao, "A micro-robot fish with embedded SMA wire actuated flexible biomimetic fin," *Sens. Actuators A, Phys.*, vol. 144, no. 2, pp. 354–360, Jun. 2008.

[2] D. R. Blidberg, "The development of autonomous underwater vehicles (AUV); a brief summary," in *Proc. IEEE ICRA*, Jun. 2001, vol. 4, no. 1, pp. 1–12.

[3] R. D. Christ and R. L. W. Sr, *The ROV Manual: A User Guide for Remotely Operated Vehicles*. London, U.K.: Butterworth-Heinemann, 2013.

[4] C. C. Lindsey. (1978). *Form, Function and Locomotory Habits in Fish*. Locomotion. [Online]. Available: https://cir.nii.ac.jp/crid/1573105975382273408

[5] P. Nilas, "A prototypical multi-locomotive robotic fish parametric research and design," in *Proc. World Congr. Eng. Comput. Sci.*, vol. 1, 2011, pp. 19–21.
[6] J. M. Anderson, K. Streitlien, D. S. Barrett, and M. S. Triantafyllou, "Oscillating foils of high propulsive efficiency," *J. Fluid Mech.*, vol. 360, pp. 41–72, Apr. 1998.
[7] J. Zhu, C. White, D. K. Wainwright, V. Di Santo, G. V. Lauder, and H. Bart-Smith, "Tuna robotics: A high-frequency experimental platform exploring the performance space of swimming fishes," *Sci. Robot.*, vol. 4, no. 34, Sep. 2019, Art. no. eaax4615.
[8] R. J. Clapham and H. Hu, "ISplash-I: High performance swimming motion of a carangiform robotic fish with full-body coordination," in *Proc. IEEE Int. Conf. Robot. Autom. (ICRA)*, May 2014, pp. 322–327.
[9] R. J. Clapham and H. Hu, "*iSplash*: Realizing fast carangiform swimming to outperform a real fish," in *Robot Fish*. Berlin, Germany: Springer, 2015, pp. 193–218.
[10] R. K. Katzschmann, J. DelPreto, R. MacCurdy, and D. Rus, "Exploration of underwater life with an acoustically controlled soft robotic fish," *Sci. Robot.*, vol. 3, no. 16, Mar. 2018, Art. no. eaar3449.
[11] Y. Bar-Cohen, "Biomimetics—Using nature to inspire human innovation," *Bioinspirations Biomimetics*, vol. 1, no. 1, pp. P1–P12, Mar. 2006.
[12] C. Guo and Z. Wang, "Design and simulations of a virtual fishlike robot actuated by a muscle model," in *Bio-Mechanisms of Swimming and Flying*. Tokyo, Japan: Springer, 2008, pp. 221–232.
[13] A. R. Chowdhury, B. Prasad, V. Vishwanathan, R. Kumar, and S. K. Panda, "Bio-harmonized dynamic model of a biology inspired carangiform robotic fish underwater vehicle," *IFAC Proc. Volumes*, vol. 47, no. 3, pp. 7258–7265, 2014.
[14] J. Liu and H. Hu, "Biological inspiration: From carangiform fish to multi-joint robotic fish," *J. Bionic Eng.*, vol. 7, no. 1, pp. 35–48, 2010.
[15] R. K. Katzschmann, A. D. Marchese, and D. Rus, "Hydraulic autonomous soft robotic fish for 3D swimming," in *Experimental Robotics*. Cham, Switzerland: Springer, 2016, pp. 405–420.
[16] L. Ma, Z. Yue, and R. Zhang, "Path tracking control of hybrid-driven robotic fish based on deep reinforcement learning," in *Proc. IEEE Int. Conf. Mechatronics Autom. (ICMA)*, Oct. 2020, pp. 815–820.
[17] S. Khan, S. Javed, N. Naeem, and I. Ali, "Performance analysis of PID and state-feedback controller on the depth control of a robotic fish," in *Proc. Int. Conf. Frontiers Inf. Technol. (FIT)*, Dec. 2017, pp. 7–11.
[18] H. Wang, C. Mi, Z. Li, N. Hou, and G. Xie, "A novel data-assisted model and discrete-time sliding mode steering controller of robotic fish," in *Proc. IEEE Int. Conf. Mechatronics, Robot. Autom. (ICMRA)*, May 2018, pp. 47–51.
[19] H. Wang, C. Mi, Z. Cao, J. Zheng, Z. Man, X. Jin, and H. Tang, "Precise discrete-time steering control for robotic fish based on data-assisted technique and super-twisting-like algorithm," *IEEE Trans. Ind. Electron.*, vol. 67, no. 12, pp. 10587–10599, Dec. 2020.
[20] M. Ye, H. Wang, A. Yazdani, S. He, Z. Ping, and W. Xu, "Discrete-time integral terminal sliding mode-based speed tracking control for a robotic fish," *Nonlinear Dyn.*, vol. 105, no. 1, pp. 359–370, Jul. 2021.
[21] X. Song, S. Gao, C. Chen, and Z. Gao, "Enhanced fireworks algorithm-auto disturbance rejection control algorithm for robot fish path tracking," *Int. J. Comput. Commun. Control*, vol. 14, no. 3, pp. 401–418, May 2019.
[22] C. Bal, G. O. Koca, D. Korkmaz, Z. H. Akpolat, and M. Ay, "CPG-based autonomous swimming control for multi-tasks of a biomimetic robotic fish," *Ocean Eng.*, vol. 189, Oct. 2019, Art. no. 106334.
[23] Z.-M. Li, X.-H. Chang, and J. H. Park, "Quantized static output feedback fuzzy tracking control for discrete-time nonlinear networked systems with asynchronous event-triggered constraints," *IEEE Trans. Syst., Man, Cybern., Syst.*, vol. 51, no. 6, pp. 3820–3831, Jun. 2021.
[24] X. Jia, D. Zhang, X. Hao, and N. Zheng, "Fuzzy H_∞ tracking control for nonlinear networked control systems in T–S fuzzy model," *IEEE Trans. Syst., Man, Cybern., B, Cybern.*, vol. 39, no. 4, pp. 1073–1079, Aug. 2009.
[25] S. Du, C. Zhou, J. Yu, and Z. Wu, "A modified line-of-sight method for path tracking applied to robotic fish," in *Proc. IEEE Int. Conf. Mechatronics Autom. (ICMA)*, Oct. 2020, pp. 809–814.
[26] J. Liu, Z. Liu, and J. Yu, "Line-of-sight based three-dimensional path following control for an underactuated robotic dolphin," *Sci. China Inf. Sci.*, vol. 64, no. 1, pp. 1–12, Jan. 2021.
[27] Y. Mu, J. Qiao, J. Liu, D. An, and Y. Wei, "Path planning with multiple constraints and path following based on model predictive control for robotic fish," *Inf. Process. Agricult.*, vol. 9, no. 1, pp. 91–99, Mar. 2022.
[28] M. Barton and C. E. Bond, *Bond's Biology of Fishes*, 3rd ed. Belmont, CA, USA: Thomson, 2007.
[29] M. J. Lighthill, "Note on the swimming of slender fish," *J. Fluid Mech.*, vol. 9, no. 2, pp. 305–317, 1960.
[30] J. Gray, *Animal Locomotion*. London, U.K.: Weidenfeld & Nicolson, 1968.
[31] F. Xie, Z. Li, Y. Ding, Y. Zhong, and R. Du, "An experimental study on the fish body flapping patterns by using a biomimetic robot fish," *IEEE Robot. Autom. Lett.*, vol. 5, no. 1, pp. 64–71, Jan. 2020.
[32] J. Yu, M. Tan, and J. Zhang, "Fish-inspired swimming simulation and robotic implementation," in *Proc. 41st Int. Symp. Robot., 6th German Conf. Robot.*, Jun. 2010, pp. 1–6.
[33] S. M. Stead and L. Laird, *The Handbook of Salmon Farming*. London, U.K.: Springer, 2002.
[34] K. J. Waldron and J. Schmiedeler, "Kinematics," in *Springer Handbook of Robotics*. Cham, Switzerland: Springer, 2016, pp. 11–36.
[35] A. N. A. Mazlan, "A fully actuated tail propulsion system for a biomimetic autonomous underwater vehicle," Ph.D. dissertation, School Eng., Aerosp. Sci., Univ. Glasgow, Glasgow, U.K., 2015.
[36] I. Eker, "Sliding mode control with PID sliding surface and experimental application to an electromechanical plant," *ISA Trans.*, vol. 45, no. 1, pp. 109–118, Jan. 2006.
[37] S. M. Amrr and A. Alturki, "Robust control design for an active magnetic bearing system using advanced adaptive SMC technique," *IEEE Access*, vol. 9, pp. 155662–155672, 2021.
[38] Z. Zuo, "Trajectory tracking control design with command-filtered compensation for a quadrotor," *IET Control Theory Appl.*, vol. 4, no. 11, pp. 2343–2355, Nov. 2010.
[39] P. Dorato, "A historical review of robust control," *IEEE Control Syst. Mag.*, vol. SM-7, no. 2, pp. 44–47, Apr. 1987.
[40] V. Utkin, "Variable structure systems with sliding modes," *IEEE Trans. Autom. Control*, vol. AC-22, no. 2, pp. 212–222, Apr. 1977.
[41] V. Utkin, J. Guldner, and J. Shi, *Sliding Mode Control in Electromechanical Systems*. Boca Raton, FL, USA: CRC Press, 2017.
[42] S. Saha, S. M. Amrr, M. U. Nabi, and A. Iqbal, "Reduced order modeling and sliding mode control of active magnetic bearing," *IEEE Access*, vol. 7, pp. 113324–113334, 2019.
[43] S. M. Amrr, A. Chakravarty, M. M. Alam, A. A. Algethami, and M. Nabi, "Efficient event-based adaptive sliding mode control for spacecraft attitude stabilization," *J. Guid., Control, Dyn.*, vol. 45, no. 7, pp. 1328–1336, Jul. 2022.
[44] S. M. Amrr, J. Ahmad, S. A. Waheed, A. Sarwar, A. S. Saidi, and M. Nabi, "Finite-time adaptive sliding mode control of a power converter under multiple uncertainties," *Frontiers Energy Res.*, vol. 10, p. 580, May 2022.
[45] S. Yu, X. Yu, and R. J. Stonier, "Continuous finite-time control for robotic manipulators with terminal sliding mode," *Automatica*, vol. 41, no. 11, pp. 1957–1964, 2003.
[46] S. P. Bhat and D. S. Bernstein, "Finite-time stability of continuous autonomous systems," *SIAM J. Control Optim.*, vol. 38, no. 3, pp. 751–766, Jan. 2000.
[47] J. K. Hedrick and A. Girard, "Control of nonlinear dynamic systems: Theory and applications," in *Controllability and Observability of Nonlinear Systems*, vol. 48. Paris, France: Encyclopedia of Life Support Systems, 2005, pp. 133–160.
[48] S. B. Niku, *Introduction to Robotics: Analysis, Control, Applications*. Hoboken, NJ, USA: Wiley, 2020.
[49] S. M. Amrr, R. Sarkar, A. Banerjee, A. S. Saidi, and M. U. Nabi, "Fault-tolerant finite-time adaptive higher order sliding mode control with optimized parameters for attitude stabilization of spacecraft," *Int. J. Robust Nonlinear Control*, vol. 32, no. 5, pp. 2845–2863, Mar. 2022.

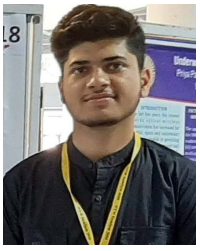

SHUBHAM SINGH received the B.Tech. degree in mechanical engineering from the Department of Mechanical Engineering, Zakir Husain College of Engineering & Technology (ZHCET), Aligarh Muslim University (AMU), Aligarh, India. He is currently pursuing the M.Tech. degree in mechanical engineering with specialization in robotics with the Indian Institute of Technology, Gandhinagar, Gujarat, India. He has published three Indian patents and two conference papers related to autonomous underwater vehicles (AUVs). His research interests include dynamics and control of autonomous underwater vehicles (AUV), remotely operated underwater vehicles (ROV), series elastic actuators (SEA) for compliant mechanisms, and biomedical devices. He is a Student Member of the Marine Technology Society, USA, and an Ex-Coordinator of the Marine Technology Society-Autonomous Underwater vehicle Club (MTS-AUV) at the ZHCET, AMU.

SAOOD AHMAD received the B.Tech. degree in mechanical engineering from the Department of Mechanical Engineering, Aligarh Muslim University, Aligarh, where he is currently pursuing the M.Tech. degree in robotics and automation. His research interests include dynamics and control design of autonomous underwater vehicles and biomedical devices.

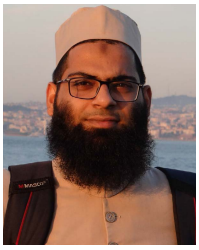

SYED MUHAMMAD AMRR (Graduate Student Member, IEEE) received the B.Tech. degree in electrical engineering and the M.Tech. degree in instrumentation and control from the Department of Electrical Engineering, Aligarh Muslim University (AMU), Aligarh, India, in 2014 and 2016, respectively, and the Ph.D. degree in control & automation from the Department of Electrical Engineering, Indian Institute of Technology Delhi (IITD), New Delhi, India, in 2021. He is currently an Early Postdoctoral Researcher with the IITD. He has published more than 40 research papers in refereed international journals and conference proceedings. Further, two international patents are also granted to his name, and he has authored a book chapter with CRC, Taylor & Francis, USA. His research interests include nonlinear control, sliding mode control, robust control, spacecraft systems, unmanned autonomous vehicles, constrained network control systems, renewable energy, and power electronics.

SALEEM ANWAR KHAN received the B.Tech. degree in mechanical engineering, the M.Tech. degree in thermal engineering, and the Ph.D. degree in the area of computational fluid dynamics and heat transfer from the Department of Mechanical Engineering, Aligarh Muslim University (AMU), Aligarh, India, in 2000, 2002, and 2011, respectively. He joined the Department of Mechanical Engineering, AMU, as an Assistant Professor, in 2007, where he has been working as a Professor, since 2020. He has completed two independent research projects with total funding of approx. 34k USD. He has published three patents on autonomous underwater vehicles (AUVs). Apart from patents, he has published books and more than 30 research articles in book, chapters, and journals of international repute. His research interests include AUVs, biomimetic fish underwater robots, heat mass transfer and fluid flow, computational fluid dynamics, and fluid-structure interaction.

NAZRUL ISLAM received the B.Sc. (Engg) degree in mechanical engineering and the M.Sc. (Engg) degree in thermal engineering from the Department of Mechanical Engineering, Aligarh Muslim University (AMU), Aligarh, India, in 1988 and 1990, respectively, and the Ph.D. degree in thermal engineering from the Department of Mechanical Engineering, Indian Institute of Technology Bombay (IITB), Mumbai, India, in 1997. He is currently working as an Associate Professor with the Department of Mechanical Engineering, King Abdulaziz University (KAU), Jeddah, Saudi Arabia. Before joining KAU, he worked as a Faculty Member with the Department of Mechanical Engineering, Jamia Millia Islamia (1996–1998) and Aligarh Muslim University (1998–2006). He has published more than 30 research papers in refereed international journals and conference proceedings. Further, he has supervised seven master's theses and several B.S. projects. His research interests include mixed convection heat transfer, CFD, nanofluidic heat transfer, and sustainable energy.

ABDULLATIF ABDULHADI GARI was born in Jeddah, Saudi Arabia, in 1970. He received the B.S. degree in mechanical engineering from King Abdulaziz University, Jeddah, in 1994, the M.S. degree in mechanical engineering from Oklahoma State University, Stillwater, OK, USA, in 1999, and the Ph.D. degree in mechanical engineering from the University of South Florida, Tampa, FL, USA, in 2006. He worked as a Teaching Assistant at King Abdulaziz University, from 1994 to 1996. He has been an Assistant Professor at the Mechanical Engineering Department, King Abdulaziz University, since 2006. He was assigned as a Vice Dean of the Engineering College at Rabigh Branch, from 2009 to 2011. He was a Visiting Professor at Villanova University for a period of ten months during 2015–2016. He has published more than 15 research papers in refereed international journals and conference proceedings. His research interests include computational fluid dynamics, heat transfer, microchannel cooling, ice melting systems, thermal storage systems, nanofluids, solar energy, and phase changing materials. He has received an award for the Best B.S. Graduation Project in the Thermal Engineering Department in 1995.

ABDULLAH A. ALGETHAMI (Member, IEEE) received the B.S. and M.S. degrees in mechanical systems production and design from King Abdulaziz University, Jeddah, Saudi Arabia, in 2002 and 2009, respectively, and the Ph.D. degree in mechanical engineering from Texas A&M University, College Station, TX, USA, in 2017. He joined Saudi Aramco, as a Student Trainee, during the 2000 and 2001 summer. Additionally, he worked with the Industrial Support Establishment (ISE) for eight years. In January 2018, he joined the Department of Mechanical Engineering, Taif University, where he is currently an Assistant Professor. His research interests include analysis, design, and real-time control of mechatronic systems, as well as control engineering and technology. He is a member of ASME.